



Multi-dimensional performance optimization of CO₂ mixture power generation system using ANN and double-helix weighting mechanism

Qingqiang Meng^a, Lihua Cao^{a,*}, Yanchao Li^b, Heyong Si^a, Yaoli Wang^a, Feng Hou^a

^a School of Energy and Power Engineering, Northeast Electric Power University, Jilin, 132012, China

^b Jilin Electric Power Co., Ltd., No. 9699, Renmin Street, Changchun, 130022, China

ARTICLE INFO

Handling editor: Dr. Q. F. Ofelia Araujo

Keywords:

Concentrated solar power
CO₂ mixed working fluid
Thermodynamic analysis
Artificial neural network
Multi-criteria performance evaluation

ABSTRACT

The use of carbon dioxide (CO₂) mixtures in the thermodynamic power cycle and its combination with the systems used for the generation of solar thermal power can significantly improve the thermal efficiency of the system and reduce costs. However, the selection of additives in mixed working fluids faces various challenges such as the inadequacy of a comprehensive evaluation system, difficulties in determining the weights of different indicators, and other issues such as a cumbersome evaluation process and high resource consumption. With this backdrop, the present paper innovatively proposed the double-helix weighting mechanism and established a two-layer structure for the 4-dimensional comprehensive evaluation system. Subsequently, by combining the multi-objective optimization of the artificial neural network surrogate model, the rapid determination of additives and operating parameters was achieved, thereby driving the comprehensive optimization of the performance of solar thermal power generation system. The results showed that through the double optimization of additives and operating parameters, the CO₂-propane system stood out with a high closeness of 0.62047, with corresponding turbine inlet pressure, temperature, and split ratio of 823.01 K, 26.374 MPa, and 0.226, respectively. Under the same operating parameters, the CO₂-propane system achieved η_t of 19.03 % and W_{net} of 45.185 MW. Compared to the CO₂ system, the value of η_t improved by 0.57 %, whereas that of W_{net} increased by 1.36 MW. In terms of economics, the LCOE and SIC were the lowest with values of 0.181 \$/kWh and 2394.77 \$/kW, respectively. In addition, the irreversible losses in the collector and high-temperature heat exchanger were significantly reduced. The η_{ex} increased to 20.44 %, which was 0.61 % higher than that of the pure CO₂ system.

1. Introduction

With its compact structure and excellent thermodynamic performance, the Brayton cycle employing supercritical carbon dioxide (sCO₂) has become an important research direction for advanced power cycles [1,2]. However, it is worth noting that the use of pure CO₂ as a working fluid faces significant technical bottlenecks in practical engineering applications. Due to the sensitivity of critical parameters to operating conditions, the state of working fluid may deviate from the supercritical region, leading to a decline in the thermal efficiency of the system [3]. Although existing studies suggest that optimizing pressure and system layout can improve the performance of the system, the resulting increase in the complexity of device and the investment costs have become key issues limiting the large-scale engineering application of this technology [4].

In recent years, the introduction of mixed working fluids to regulate

the critical properties of CO₂, thereby reducing its sensitivity to operating conditions, has been regarded as an effective pathway to overcoming various limitations to the performance of power cycles. Bian et al. [5] analyzed the performance of power cycles involving transcritical CO₂-mixed working fluids through thermodynamic modeling and found that the mixed working fluids of CO₂-propane and CO₂-hydrogen sulfide (H₂S) could increase the thermal efficiency of pressurized water reactors and high-temperature reactors to 33.07 % and 46.07 %, respectively. Ma and Niu et al. [6,7] were the first to use a thermodynamic analysis based on the optimum split ratio to evaluate the potential application of CO₂-mixed working fluids in solar power tower (SPT) systems. They analyzed the impact of key parameters on the thermal performance of the system, and showed that, compared to pure CO₂, the thermal and exergy efficiencies of CO₂-propane were improved by 2.34 % and 1.51 %, respectively, compared to pure CO₂. Illyés et al. [8] experimentally validated the feasibility of CO₂-hexfluoro benzene

* Corresponding author.

E-mail address: clh320@126.com (L. Cao).

(C₆F₆)-mixed working fluid in a transcritical cycle, confirming that it could reduce condensation pressure and maintain high-temperature stability, thus offering a new solution for generating solar thermal power. Lang et al. [9] conducted thermodynamic analysis and found that the mixed working fluid of CO₂-SO₂ could effectively enhance the power output of hypersonic aircraft's power generation systems under limited cooling source conditions (with a power output of 159 kJ/kg of fuel), making it the optimum choice of fluid in the power generation systems of hypersonic aircrafts. Luo et al. [10] proposed a floating critical point adjustment method, which enhanced the annual efficiency of the sCO₂ cycle by 7–10.9 % under off-design conditions, and verified the applicability of this method for generating solar thermal power. Liang et al. [11] developed a novel solar-liquified natural gas (LNG) cold energy hybrid system using R290-CO₂ as the working fluid, achieving a 15.6 % increase in exergy efficiency and a 10.7 % reduction in costs. These studies suggest that using mixed working fluids is an effective method for improving the efficiency of thermal cycle, especially for optimizing and retrofitting the existing systems.

The addition of additives to CO₂ greatly enhances the thermodynamic performance of the system. However, its use often leads to changes in the operating and maintenance costs of the system. As a result, many researchers have gradually shifted towards double optimization of both the technology and the economy to establish a balance between the technical performance and the corresponding economic costs [12]. Ma et al. [13] studied the application of a working fluid consisting of a mixture of CO₂ and rare gases in the Brayton cycle, and found that the mixed working fluid could effectively improve the thermal efficiency of the system. Cheng et al. [14] used a multi-objective optimization method and found that the mixed working fluid of CO₂-(krypton) Kr could increase the thermal efficiency of the supercritical Brayton cycle to 46 %, reduce costs by 6.7 %, and decrease the volume of equipment by 11.7 %. Dai et al. [15] investigated a transcritical CO₂ combined heating and cooling system using hydrocarbon mixtures through thermodynamic modeling and multi-objective optimization, and reported that the mixed working fluid of R290-R601 improved the coefficient of performance (COP) of the system by 8.2 % and reduced the lifecycle carbon emissions by 9.31 %. Yang et al. [16] explored the impact of various working fluids' mixing ratios on the thermal efficiency and economics of Brayton cycle, and showed that CO₂-fluoroethane exhibited the most favorable economic performance, achieving optimum performance under different operating conditions, especially at high temperatures, and significantly improving efficiency while reducing the operating costs of the system. Khan et al. [17] integrated an ejector-assisted transcritical CO₂ refrigeration (ETCR) subsystem and a flash tank with a compression absorption refrigeration (FCAR) subsystem, combining power generation and cooling systems. The results of their study showed that the peak thermal efficiency and exergy efficiency of the system reached 61.8 % and 65.76 %, respectively. Xu et al. [18] systematically assessed seven organic candidates for the application of organic Rankine cycle (ORC) through a hierarchical decision model integrating Pareto optimization. Their analysis revealed that gains in thermodynamic performance were correlated with elevated component ratios, and attributed to enhanced modulation of phase behavior at higher concentrations of organic fluids.

Based upon the above literature review, it is evident that existing selection systems for various additives have significant shortcomings. Most studies focus on the analysis of the thermodynamic performance from a single dimension, with only a few works combining thermodynamic performance and economics for the overall performance evaluation of the system. However, there is still a lack of effective evaluation mechanisms for scientifically quantifying the non-technical indicators such as environmental and social benefits. When determining the weights of different indicators, most methods rely on either subjective or objective weight calculation, making it difficult to achieve reasonable distribution of weight. Furthermore, the calculation process in the selection of additives and the optimization of parameters is complex and

resource-intensive, remaining a bottleneck that restricts the efficiency of the selection of working fluid and the optimization of various parameters for a thermal power cycle.

To address these shortcomings, the present paper innovatively proposes the double-helix weighting mechanism, overcoming the limitations of single-weighting methods. Based on this, a 4-DCES integrating technical performance, economics, environmental performance, and social responsibility is established. Subsequently, for a concentrating solar power (CSP) system, an artificial neural network-based surrogate model is developed, enabling the rapid and efficient optimization of types of additives and operating parameters, and achieving multi-dimensional performance optimization of the CSP system using the proposed 4-DCES. The present study not only fills the gap in existing evaluation systems regarding dimensional completeness and rationality of weighting but also addresses the issues of complex calculation processes and high resource consumption. Additionally, the study provides new insights for the thermodynamic analysis of the differences in the performances of various mixed working fluids. Fig. 1 shows the computational flowchart for the present study.

The paper is organized such that Section II describes the assumptions and mathematical models for each component of the system, including evaluation metrics for technical performance, economic benefits, environmental sustainability, and social impact. Section III elaborates the research methodology by first constructing an artificial neural network surrogate model that is based on a double-spiral weighting mechanism, and then employing the NSGA-II algorithm for multi-objective optimization. Finally, the optimized formulation for the additive and the optimized operating parameters for the system are determined through an entropy-weighted TOPSIS coupled decision-making approach. Section IV conducts a detailed comparative analysis, examining the differences in the performances of systems employing pure CO₂ and the mixed working fluids from both thermodynamic and exergy efficiency perspectives. Lastly, Section 5 presents the conclusions drawn from the analysis conducted in the work.

2. System modeling

2.1. System layout and assumptions

The cycle system consisted of a solar thermal collection system, a thermal storage system, and a Brayton cycle system, as shown in Fig. 2. When the output of the concentrating solar power (CSP) system exceeded demand, the thermal storage system stored heat and released power during peak loads or at night, thus ensuring power supply for long-durations. The thermal storage system used a direct double-tank energy storage method, with molten salt serving as both the heat transfer medium and the storage material. Table 1 lists the physical properties of the molten salt used in the current work [19].

The mathematical model was established based on the following assumptions.

- (1) The system operated under steady-state conditions.
- (2) No chemical reactions occurred in the mixture during the operation of the system.
- (3) Cooling air used in the precooler was under ambient conditions.
- (4) There was no energy loss in mechanical transmission.

2.2. Mathematical model

2.2.1. Thermodynamic model

(1) Concentrating Solar Power System

The heat exchange process of the solar collector can be represented by Equation (1).

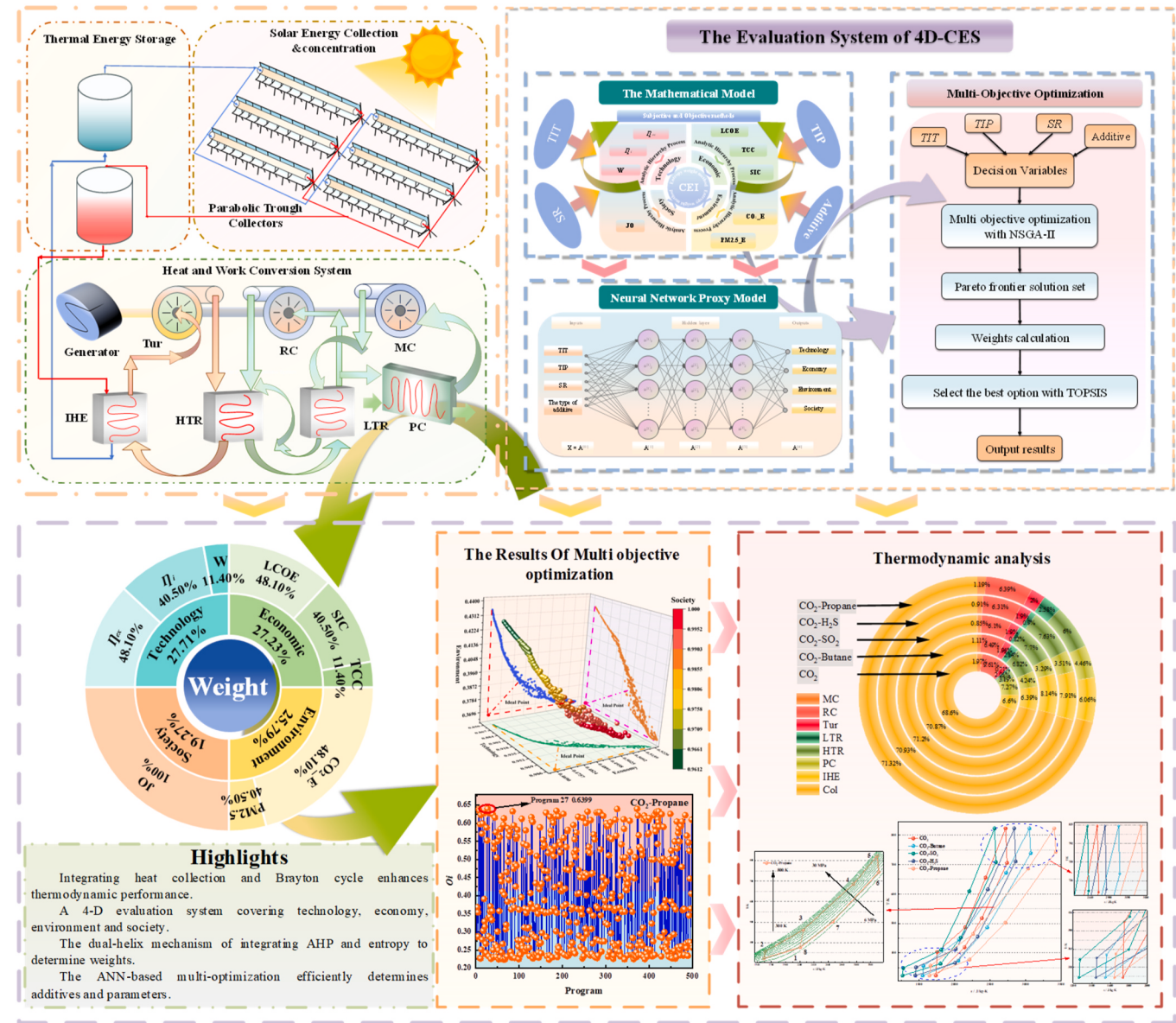


Fig. 1. Computational flowchart.

$$Q_{col} = DNI \cdot A_p \cdot \eta_{col} = m_{salt} \cdot C_{p,salt} \cdot \Delta T_{salt} \quad (1)$$

where DNI is the solar radiation intensity (W/m^2), A_p represents the total area of the solar collector, η_{col} is the collector efficiency, m_{salt} is the mass flow rate of the molten salt, $C_{p,salt}$ is the specific heat capacity of the molten salt at the average temperature, and ΔT represents the increase in the temperature of the molten salt during the heat transfer process.

The efficiency of the collector is calculated using Equation (2).

$$\eta_{col} = \eta_0 - U_l \cdot \frac{T_{mean} - T_{Ambt}}{DNI \cdot \cos(\theta)} \quad (2)$$

where η_0 is the optical efficiency of the collector, having a value of 0.7, U_l is the loss coefficient, with a value of 0.1 [20]. T_{mean} is the average temperature, T_{Ambt} is the ambient temperature, and θ is the incidence angle of the solar beam.

(2) Heat storage and exchange system

The energy balance of the thermal storage system is given by Equation (3).

$$Q_{IHE} \cdot t_{discharge} = m_{salt} \cdot C_{p,salt} \cdot \Delta T_{salt} \cdot t_{change} \quad (3)$$

where Q_{IHE} is the total heat exchange of the heat source exchanger, and t_{change} and $t_{discharge}$ represent the time points for heat storage and discharge of heat in the thermal storage system, respectively.

(3) Compressor and Turbine Model

The specific enthalpy and pressure at the outlet can be calculated using Equations (4)–(7).

$$h_{com,out} = h_{com,in} + \frac{h_{com,out,s} - h_{com,in}}{\eta_{com}} \quad (4)$$

$$P_{com,out} = PR_{com} \cdot P_{com,in} \quad (5)$$

$$h_{tur,out} = h_{tur,in} - \eta_{tur} \cdot (h_{tur,in} - h_{tur,out,s}) \quad (6)$$

$$P_{tur,out} = \frac{P_{tur,in}}{PR_{tur}} \quad (7)$$

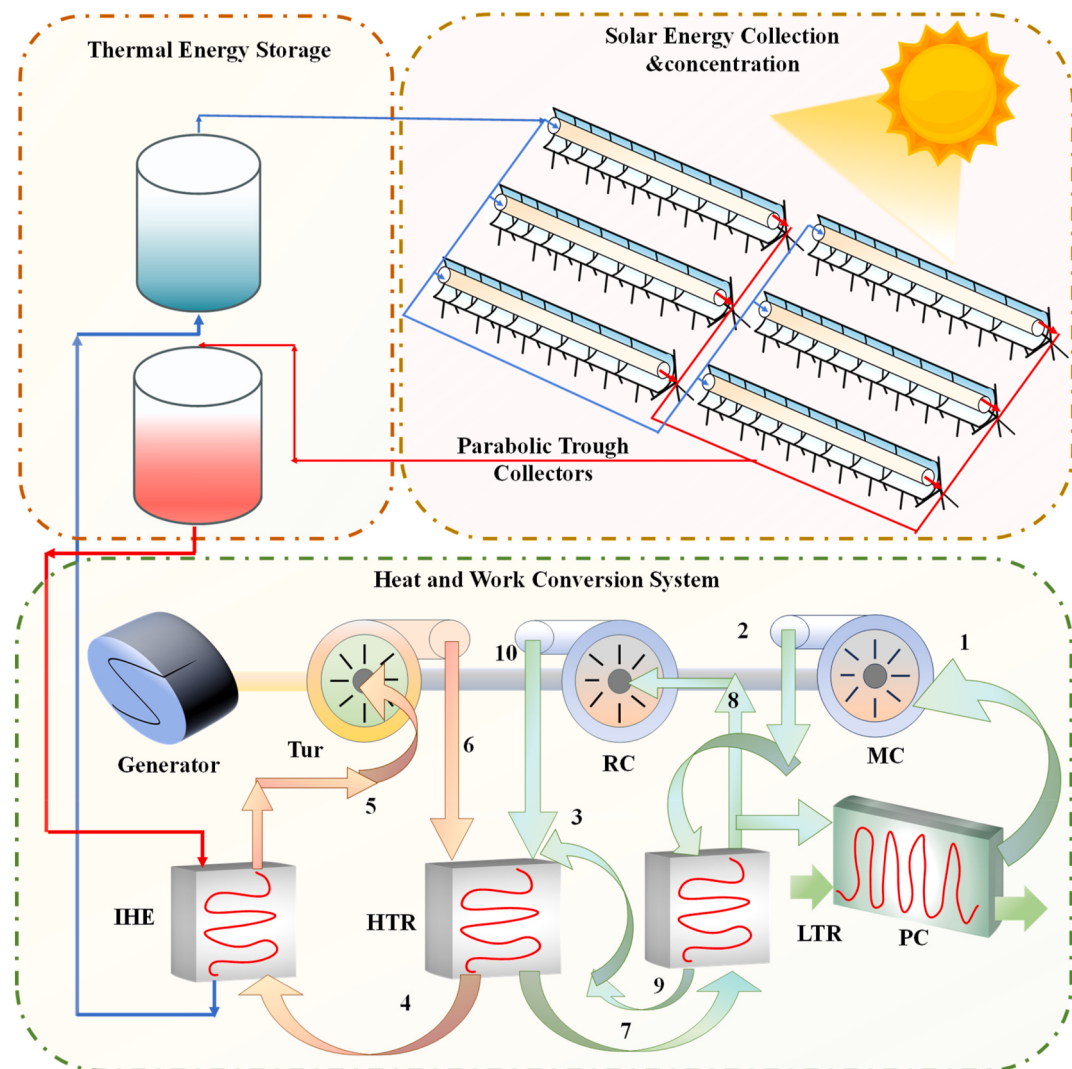


Fig. 2. System layout.

Table 1
Physical parameters of molten salts [19].

Molten salts	Molten chloride salt
Constituent	8.1 wt% NaCl + 31.3 wt% KCl + 60.6 wt% ZnCl ₂
Melting point/K	472.15
Upper temperature limit/K	1173.15
Specific heat capacity/ J·kg ⁻¹ K ⁻¹	917
Viscosity/Pa·s	152.4·exp(-T/56.03) + 0.06·exp(-T/235.79 + 0.003)

where h is the enthalpy, η is the efficiency, P is the pressure, and PR is the pressure ratio. The subscript ‘in’ and ‘out’ refer to the inlet and outlet, respectively, whereas com denotes a compressor, and tur denotes a turbine.

The output power of turbine and compressor can be expression by Equations (8) and (9), respectively.

$$W_{com} = m_{com} \cdot (h_{com,out} - h_{com,in}) \quad (8)$$

$$W_{tur} = m_{tur} \cdot (h_{tur,in} - h_{tur,out}) \quad (9)$$

where W represents the power consumption or output of the rotating equipment.

The thermal efficiency of the power cycle is given by Equation (10).

$$\eta_{pc} = \frac{W_{tur} - W_{MC} - W_{RC}}{Q_{IHE}} \quad (10)$$

The total system efficiency is given by Equation (11).

$$\eta_i = \eta_{col} \times \eta_{pc} \quad (11)$$

The specific work reflects the energy conversion efficiency, and is given by Equation (12).

$$W = \frac{W_{net}}{m} \quad (12)$$

(4) Heat Exchanger Model

The conservation of energy is represented by Equations (13)–(15) [21].

$$h_{HTR,hin} - h_{HTR,hout} = h_{HTR,cout} - h_{HTR,cin} \quad (13)$$

$$h_{LTR,hin} - h_{LTR,hout} = SR \cdot (h_{LTR,cin} - h_{LTR,cout}) \quad (14)$$

$$h_{HTR,cin} = SR \cdot h_{HTR,cout} + (1 - SR) \cdot h_{out,RC} \quad (15)$$

$$\varepsilon_{HTR} = \frac{(T_{HTR,hin} - T_{HTR,hout}, T_{HTR,cout} - T_{HTR,cin})_{\max}}{T_{HTR,hin} - T_{HTR,cin}} \quad (16)$$

$$\varepsilon_{LTR} = \frac{(T_{LTR,hin} - T_{LTR,hout}, T_{LTR,cout} - T_{LTR,cin})_{\max}}{T_{LTR,hin} - T_{LTR,cin}} \quad (17)$$

where, *HTR* and *LTR* represent the high-temperature and low-temperature recuperators, respectively, and *SR* denotes the split ratio. The subscripts *hin* and *hout* are the inlet and outlet on the hot side of the reheat, respectively, and *c_{in}* and *c_{out}* are the cold side's inlet and outlet of the reheat, respectively.

Based on the mathematical model of the solar thermal power generating system, the calculation process first set an initial value for the cold side's inlet temperature of the low-temperature heat exchanger. Then, using the bisection method, the temperature value was iteratively adjusted. After each iteration, the actual temperature at that point was calculated. When the absolute error between the calculated value and the assumed value became less than 1×10^{-4} , the iteration was terminated.

(5) Exergy Loss Model

The radiation exergy incident on the mirror surface from the sun is calculated by Equation (18) [22].

$$E_{in} = Q_s \cdot \left[1 - \frac{4}{3} \cdot \left(\frac{T_{Ambt}}{T_s} \right)^4 + \frac{1}{3} \cdot \left(\frac{T_{Ambt}}{T_s} \right)^4 \right] \quad (18)$$

$$Q_s = DNI \cdot A_p \cdot \eta_0 \quad (19)$$

where *T_{Ambt}* is the ambient temperature and *T_s* is the solar surface temperature (with value of 5800K).

The total exergy efficiency is given by Equation (20).

$$\eta_{ex} = \frac{W_{net}}{E_{in}} \quad (20)$$

The exergy of each state in the system is given by Equation (21).

$$E_i = m \cdot [(h_i - h_0) - T_0 \cdot (s_i - s_0)] \quad (21)$$

where *E* represents the exergy, and 0 refers to the parameters of the reference state. In this study, the reference state was represented by the temperature and pressure of 298.15 K and 0.1 MPa, respectively. The exergy loss of each component in the system is calculated, and presented in Table 2.

2.2.2. Economic model

Total capital cost (TCC), levelized cost of electricity (LCOE), and specific investment cost (SIC) are used to evaluate the economic performance of the power cycle using various CO₂ mixtures working fluids.

$$TCC = TDC + TIC \quad (22)$$

$$LCOE = \frac{TDC \cdot CRF + TIC}{t \cdot W_{net}} \quad (23)$$

Table 2
Exergy loss of various components [6].

Components	Equations
MC	$I_{MC} = W_{MC} - (E_2 - E_1)$
RC	$I_{RC} = W_{RC} - (E_{10} - E_8)$
Turbine	$I_{Tur} = W_{Tur} - (E_5 - E_6)$
HTR	$I_{HTR} = ((E_6 - E_7) - (E_4 - E_3))$
LTR	$I_{LTR} = (E_7 - E_8) - (E_9 - E_2)$
IHE	$I_{IHE} = (E_{13} - E_{14}) - (E_5 - E_4)$
Cooler	$I_{Cool} = (E_1 - E_8) - (E_{11} - E_{12})$

Table 3
Costs of individual pieces of equipment [25–29].

Cost	Subitem	Equations
Total direct cost (TDC)	RC	$Z_{k,RC} = \left(\frac{71.1 \cdot SR \cdot m}{0.92 - \eta_{com}} \right) PR \cdot \ln(PR)$
	MC	$Z_{k,MC} = \left(\frac{71.1(1 - SR) \cdot m}{0.92 - \eta_{com}} \right) PR \cdot \ln(PR)$
	Turbine	$Z_{k,Tur} = \left(\frac{479.34 \cdot m}{0.93 - \eta_{tur}} \right) \ln(PR)(1 + e^{(0.036 \cdot T_{in} - 54.4)})$
	IHE/HTR/LTR	$Z_{k,i} = 2681A_k^{0.59}$
	Cooler	$Z_{k,i} = 2143A_k^{0.514}$
	solar collector	$Z_{sc} = 150\$/m^2$
	HTF system	$Z_{HTF} = 14.28\% \text{ of } Z_{sc}$
	Cost of operation and maintenance the system	$Z_{COM} = \gamma \cdot Z_{k,i} \quad \gamma = 0.15$
	Land preparation costs	$Z_{LP} = 5.7\% \text{ of } Z_{sc}$
	Potential costs	$Z_P = 10\% \text{ of } Z_{sc} + Z_{HTF} + Z_{LP}$
Total indirect cost (TIC)	Engineering, construction, and procurement cost	$Z_{EPC} = 10\% \text{ of } Z_{TDC}$

$$CRF = \frac{i \cdot (1+i)^{LT}}{(1+i)^{LT} - 1} \quad (24)$$

$$SIC = \frac{TCC}{W_{net}} \quad (25)$$

$$Z_{K,2021} = Z_{K,2001} \frac{CEPCI_{2021}}{CEPCI_{2001}} \quad (26)$$

where *i* is the interest rate (set at 0.12), *t* is the annual operating hours (taken as 2600 h), and *LT* is the system's lifespan (set to 20 years) [23] (see Table 3). The chemical engineering plant cost index (CEPCI) for the years 2021 is 397 [24].

The heat exchange area of the heat exchanger is given by Equation (27).

$$A = \frac{Q}{U \cdot \Delta T_m} \quad (27)$$

where *Q* is the heat transfer capacity of the heat exchanger, *U* is the calculated heat transfer coefficient, and ΔT_m is the logarithmic mean temperature difference. Values of *U* and ΔT_m can be calculated using Equations (28) and (29), respectively [30,31].

$$\frac{1}{U} = \frac{1}{\alpha_h} + \frac{\delta}{\lambda} + \frac{1}{\alpha_c} \quad (28)$$

$$\Delta T_m = \frac{\Delta T_{max} - \Delta T_{min}}{\ln \Delta T_{max} / \Delta T_{min}} \quad (29)$$

where, λ is the thermal conductivity, δ is the thickness, and α denotes the heat transfer coefficient, which can be calculated by Equation (30).

$$\alpha = \lambda N u / D_h \quad (30)$$

where *D_h* is the hydraulic diameter and *Nu* is the Nusselt number, which can be expressed by Equation (31).

$$Nu = \begin{cases} Nu = 4.089, & Re < 2300 \\ Nu = 4.089 + \frac{Nu_{Re=5000} - 4.089}{5000 - 2300} (Re - 2300), & 2300 \leq Re < 5000 \\ Nu = \frac{f_c (Re - 1000) Pr}{8 [1 + 12.7 (Pr^{2/3} - 1) \sqrt{f_c / 8}]}, & Re \geq 5000 \end{cases} \quad (31)$$

$$f_c = \left(\frac{1}{1.8 \log Re - 1.5} \right)^2 \quad (32)$$

where Re represents the Reynolds number, Pr is the Prandtl number, and f_c denotes the friction factor.

2.2.3. Environmental model

The main pollutants emitted included CO_2 and PM2.5, and their intensities are calculated using Equations (33) and (35), respectively.

$$\text{CO}_2\text{-}E = \frac{\text{CO}_{2,\text{tol}}}{LT \cdot W_{\text{net}} \cdot t} \quad (33)$$

$$\text{CO}_{2,\text{tol}} = \sum_{k=1}^M \text{CO}_{2,\text{mat}} + \text{CO}_{2,\text{ele}} \quad (34)$$

$$\text{PM2.5}\text{-}E = \frac{\text{PM2.5}_{\text{tol}}}{LT \cdot W_{\text{net}} \cdot t} \quad (35)$$

$$\text{PM2.5}_{\text{tol}} = \sum_{k=1}^M \text{PM2.5}_{\text{mat}} + \text{PM2.5}_{\text{ele}} \quad (36)$$

where $\text{CO}_2\text{-}E$ and $\text{PM2.5}\text{-}E$ represent the CO_2 and PM2.5 emissions per unit of electricity, respectively, $\text{CO}_{2,\text{mat}}$ and $\text{PM2.5}_{\text{mat}}$ represent the CO_2 and PM2.5 emissions from the materials required during the construction of k -th component, respectively, and $\text{CO}_{2,\text{ele}}$ and $\text{PM2.5}_{\text{ele}}$ represent the CO_2 and PM2.5 emissions during the consumption of electricity respectively. The emissions of environmental pollutants in each stage are presented in Tables 4–6.

2.2.4. Society impacts

The construction of solar thermal power plants and related supporting facilities will create more job opportunities for the communities [35]. The employment opportunities, representing the social indicator, can be calculated by Equation (37) [36].

$$JO = \lambda_{\text{grid}} E_{\text{nom}} + \lambda_{\text{csp}} Q_{\text{csp}} \quad (37)$$

where λ_{grid} and λ_{csp} represent the grid capacity factor and the CSP capacity factor, with corresponding values of 0.61 and 0.38, respectively [37], and Q_{csp} and E_{nom} represent the power generation capacity of CSP and the nominal capacity of the power plant, respectively.

2.3. Validation

Based on the proposed mathematical model, a CO_2 Brayton cycle model was established using the software package of MATLAB. The

Table 5
Electricity emission factors for different pollutants [33].

Pollutant	Emission (g/kWh)
CO_2	968
PM2.5	3.4

accuracy and effectiveness of the proposed model, were assessed. To this end, same working fluid and model parameters as those reported in Xu [38] were used. The results were compared with Xu's findings [38]. Fig. 3 illustrates the agreement of computed results with the literature findings, with the maximum error being less than 2.5 %. This confirms the accuracy of the model used in the present study.

3. Comprehensive optimization of the performance of the solar thermal power system based on ANN

Although adding different types of additives to CO_2 can enhance the conversion efficiency of a plant, their impact on the thermodynamic performance, economics, environmental sustainability, and social benefits from the system shows varying characteristics. Therefore, by selecting appropriate additives and optimizing operating parameters, the overall performance of the solar thermal power generating system can be improved. Based on this, the present section first determined five candidate additives according to the NIST database. Then, using the double-helix weighting mechanism, an artificial neural network surrogate model was established with random data generated by a mathematical model. Next, the NSGA-II multi-objective optimization algorithm was used to obtain the Pareto front solutions under the given constraints. Finally, the entropy-weighted TOPSIS method was used to determine the optimum type of additive and optimum operating parameters for the system. Fig. 4 shows the schematic of the specific calculation process.

The schematic of the double-helix weighting mechanism is shown in Fig. 5. Its core lied in constructing a collaborative framework that integrated the analytic hierarchy process (AHP) and the information entropy method. This mechanism relied on a double-layer framework and achieved the scientific integration and balance of the four-dimensional indicators of 'technical feasibility, economic rationality, environmental compatibility, and social responsibility' through the spiral interaction. On one spiral line, the AHP method quantified the relative importance between the lower-level indicators, assigning subjective weights driven by expert knowledge, and initially aggregated them to form the upper-level indicators. Meanwhile, on another spiral line, the entropy weight method calculated the values for information entropies of the indicators based on the objective distribution characteristics of the underlying data, calibrating and objectively correcting the initial

Table 4
 CO_2 , PM2.5 emissions, and electricity consumption during the acquisition of raw materials.[32]

Material	Pollutant emission (g/kg)		Electricity Consumption(kWh/kg)
	CO_2	PM2.5	
Steel	2000	15	1.7
Aluminum	25800	290	36.1
Copper	1900		1.8
PVC	247	2.2	21.9
Glass	132.3	7	0.6

Table 6
Material and electricity consumption per component during construction.^[34]

Component	Material (kg/kW)					Electricity consumption (kWh/kW)
	Steel	Aluminum	Copper	PVC	Glass	
Collector	2.5	1.13		4.73	0.8	5.9
TES	1					1
Power	15.52					9.96

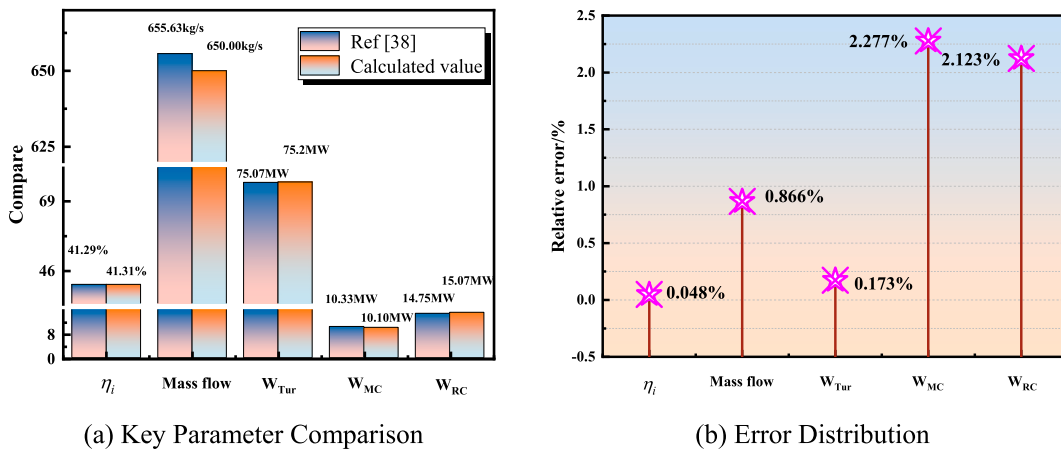


Fig. 3. Comparison of Calculation Results with literature.

weights derived from AHP, and effectively suppressing human subjective bias. These two spiral lines were not simply connected in series, rather engaged in continuous interaction. Once the lower-level related indicators were assigned weights by AHP to form the four-dimensional upper-level indicators, the entropy weight method acted on these upper-level indicators, calculating their objective weights and constructing a comprehensive evaluation index. Finally, based on the optimized weights formed by the joint action of double helix, the TOPSIS method was used to calculate the closeness of different schemes, achieving decision-making based upon multi-objective optimization. The entire mechanism functioned similar to the DNA double helix, where subjective and objective methods supported each other, collaboratively driving the scientific and balanced evaluation results.

3.1. Preliminary selection of additives

In the selection of additives, various factors such as operational parameter constraints, thermodynamic stability, low corrosiveness, and environmental safety must be comprehensively considered. Among them, hydrocarbon mixtures can be removed from the flammable range by mixing with inert gases in proportions greater than 30 % by mass [39, 40]. Based on the NIST database, six additives were initially selected. After mixing with CO₂ in a certain ratio, the variation trend of the critical parameters of the resulting mixture was obtained, as shown in Fig. 6. Although the additive of cyclohexane improved the thermodynamic performance of the working fluid, its critical pressure increased by 42 % with the increase in its mass fraction, indicating its poor stability. Therefore, five other candidates were selected for being additives, and included butane, SO₂, COS, H₂S, and propane. It is worth noticing

that although H₂S, SO₂, and COS have certain corrosive properties and safety hazards, their application as alternative working fluid to CO₂ under high-temperature conditions remains feasible, which is a courtesy of advanced sealing technologies, comprehensive regulations for their use, and sound safety management practices [38]. Moreover, H₂S can significantly increase the critical temperature and enhance the specific heat capacity of the working fluid in high-temperature regions. Moreover, by optimizing the slope of the density-temperature curve, SO₂ and COS can effectively reduce the power consumption of the compressor [4, 41]. This makes H₂S, SO₂, and COS particularly attractive as candidates for being working fluids.

3.2. Data-driven artificial neural network surrogate model

Section 2 provides the relevant evaluation indicators for the system, which are classified into the categories of technical, economic, environmental, and social indicators. The weights of the lower-level indicators were determined using AHP. These weights were then aggregated to form the four categories of technical, economic, environmental, and social indicators. The main steps of AHP included defining the hierarchical structure, assigning weights to the criteria and sub-criteria, allocating weights to the alternative solutions, and calculating the final scores [42]. Among them, pairwise comparisons of indicators are the key step. Furthermore, and the importance levels were assessed based on the scale provided in Table 7. After obtaining the relative importance distributions of different indicators (as shown by the data presented in Table 8), consistency was evaluated using Equations (38) and (39) [42], with a consistency ratio of less than 0.1. Finally, the weights of each indicator were determined, as shown by the data

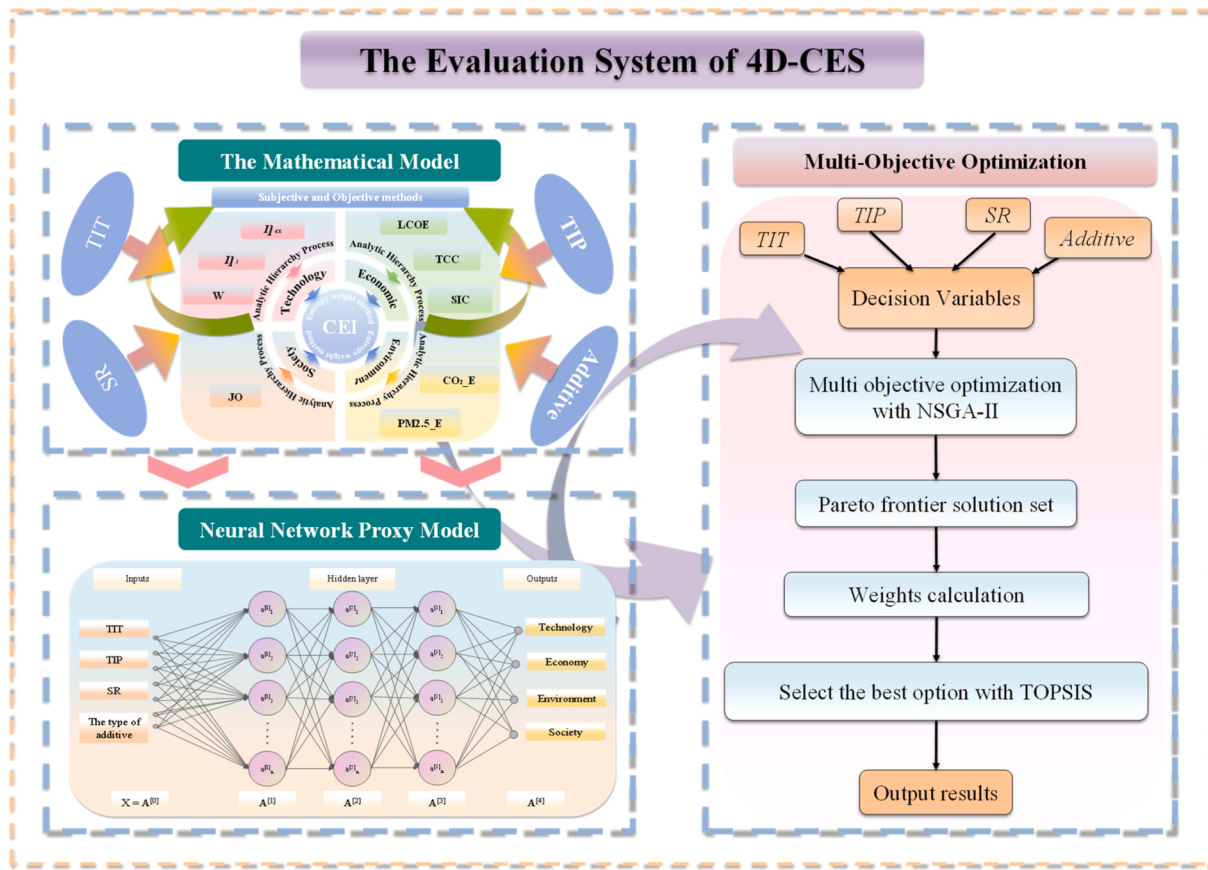


Fig. 4. The calculation process of 4D-CES evaluation system.

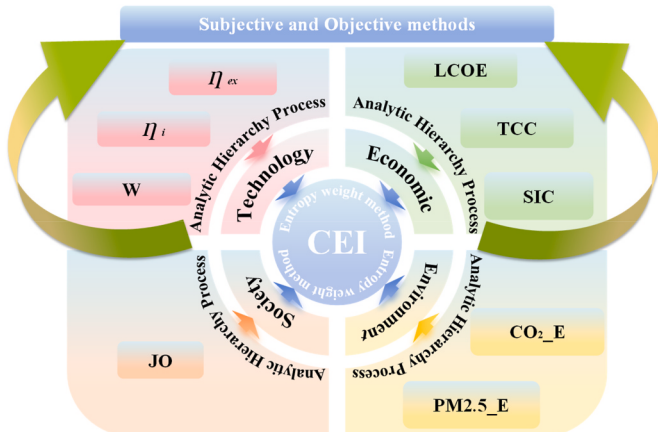


Fig. 5. The Schematic Diagram of double-helix weighting mechanism.

presented in Table 9.

$$CR = \frac{CI}{RI} \quad (38)$$

$$CI = \frac{(\lambda_{\max} - n)}{(n - 1)} \quad (39)$$

Data presented in Table 9 shows the weight distribution of each indicator. In terms of technology, the efficiency of the system had the highest weight at 48.10 %, followed by thermal efficiency at 40.50 %, while the weight of specific work was the lowest at only 11.40 %. This indicated that in the comprehensive evaluation system, the

technological indicators placed more emphasis on the utilization of energy quality. In terms of economics, the LCOE had the highest weight at 48.10 %, followed by SIC at 40.50 %, and TCC at 11.40 %. This weight distribution indicated that LCOE had the most significant impact on the economic feasibility of the system, followed by SIC and TCC [43,44]. In terms of environmental impact, the weight of CO₂ emissions was 83.30 %, which was much higher than PM2.5 (16.70 %). This was due to the reason that, in solar thermal systems, PM2.5 was mainly concentrated during the construction phase and could be controlled through dust removal technologies. However, the reduction of CO₂ emissions is more critical [45]. In terms of social benefits, social responsibility held a 100 % weight.

After determining the four-dimensional indicators, solving the power generating system that used the mixed working fluids based on the proposed mathematical model became a complex process. In the multi-parameter optimization of the solar thermal power generating system, with its nonlinear mapping capability, the artificial neural network surrogate model can significantly reduce the computational dimensionality by compressing the time for computing from the minute level to millisecond level. This effectively supports the efficient iteration of multi-objective optimization algorithms such as NSGA-II, providing an efficient solution for the optimization of complex systems [46,47]. The artificial neural network grid model is shown in Fig. 7. Using random functions, 500 sets of random data were generated for the power generating system employing the CO₂ mixed working fluids. For each working fluid, the first 400 sets of data served as the training dataset, while the remaining 100 sets were used as the testing dataset, resulting in a total of 2500 datasets. The input variables included TIT, TIP, SR, and the type of additive, while the output variables were the technical, economic, environmental, and social indicators.

In the calculation process, the training and testing datasets were split

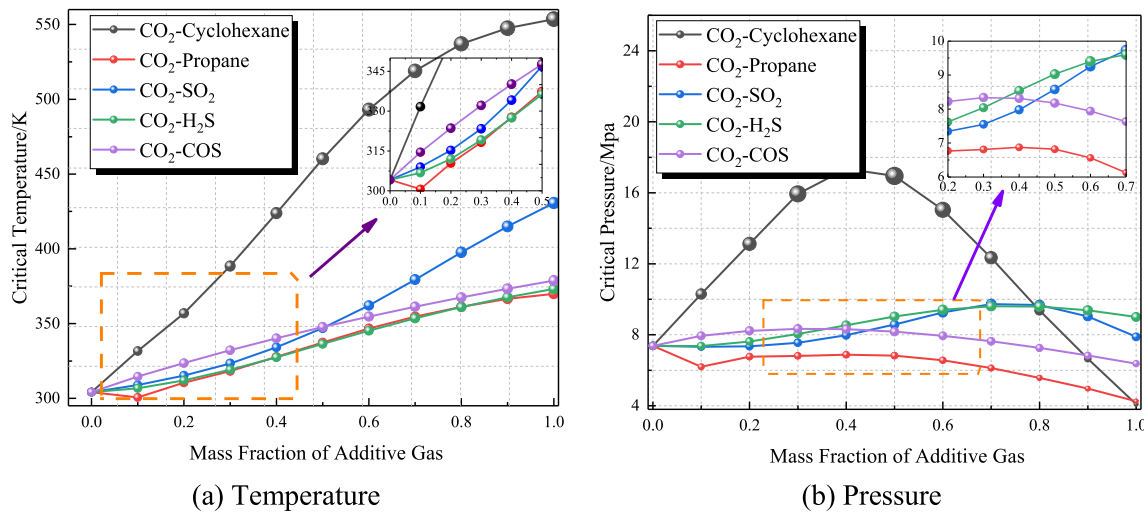


Fig. 6. Variation of critical parameters with the mass fraction of additives.

Table 7
Scale of importance in AHP.

Scale Value	Importance Degree
1	Equal priority
3	Slightly more important
5	Strong important
7	Very Strong Importance
9	Extreme Importance
2, 4, 6, 8	Intermediate values

into an 80 %–20 % ratio. After normalizing the input and output data, a three-hidden-layer BP neural network was constructed. The number of training epochs was set to 1000, with a learning rate of 0.01. The convergence error was required to be less than 1×10^{-8} . Table 10 presents the relevant settings for the model. The predicted results were validated using mean squared error. Fig. 8 shows the distribution of predicted results against the sample data. The results showed that the R^2

values for each output were close to 1, indicating that the model was reliable.

3.3. Multi-objective optimization

The surrogate model obtained using ANN employed the multi-objective optimization algorithm of NSGA-II, with technical, economic, environmental, and social indicators being the optimization objectives. In the calculation process, the algorithm of NSGA-II was used to handle the four-dimensional objective conflicts (maximizing the technical and social indicators while simultaneously minimizing the economic and environmental indicators). The elitism strategy and crowding distance operator of NSGA-II ensured the distribution and convergence of Pareto solution set [48]. This effectively guaranteed the reliability and efficiency of the computation. The decision variables were TIT, TIP, SR, and the type of additive. The parameters used for NSGA-II algorithm are presented in Table 11 [49].

The multi-objective optimization model is defined by Equation (40),

Table 8
Judgment matrix among different indicators.

Criteria	Technology			Economy			Environment		Social	
	η_{ex}	η_i	W	LCOE	SIC	TCC	CO_2_E	PM2.5	JO	
Technology	η_{ex}	1	1	5						
	η_i	1	1	3						
	W	1/5	1/3	1						
Economy	LCOE			1	1	5				
	SIC			1	1	3				
	TCC			1/5	1/3	1				
Environment	CO_2_E						1	5		
	PM_2.5						1/5	1		
Social	JO								1	

Table 9
Weight distribution of each indicator.

Dimension	Indicator	Indicator weight (%)
Technology	η_{ex}	48.10 %
	η_i	40.50 %
	W	11.40 %
Economy	LCOE	48.10 %
	SIC	40.50 %
	TCC	11.40 %
Environment	CO ₂ E	83.30 %
	PM2.5	16.70 %
Social	JO	100 %

whereas the constraints for the decision variables are given by Equation (41).

$$\begin{cases} \max Tec(TIP, TIT, SR, N) \\ \min Eco(TIP, TIT, SR, N) \\ \min Env(TIP, TIT, SR, N) \\ \max Soc(TIP, TIT, SR, N) \end{cases} \quad (40)$$

$$\begin{cases} 15MPa < TIP < 28MPa \\ 623.15K < TIT < 823.15K \\ 0.1 < SR < 0.5 \\ 1 \leq N \leq 5 \end{cases} \quad (41)$$

where TIP, TIT, and SR represent the turbine's inlet pressure, temperature, and split ratio, respectively, and N is an integer between 1 and 5, representing the types of additives, which are CO₂, butane, SO₂, COS, H₂S, and propane.

Fig. 9 shows the Pareto front solution set obtained from the ANN surrogate model. The three axes in Fig. 9 represent the system's technical, economic, and environmental performances, while the color variation reflects the trend of social benefits. Each solution on the Pareto front represents a balance point, meaning that no single objective can be improved without sacrificing other objectives. The results showed that there was a significant positive correlation between the technical and social indicators, indicating that technological innovation was often accompanied by an improvement in social benefits. However, this positive relationship was achieved at the cost of sacrificing economic and environmental performances. More specifically, the peak value of the technical indicator corresponded to an economic indicator of 0.5211

and an environmental indicator of 0.3677. This further revealed that technological breakthroughs often led to increased costs and environmental burdens. Additionally, when focusing on bi-objective optimization, the Pareto front for the technical and economic objectives formed a convex curve, with the optimum solutions concentrated within the ranges of 0.95–0.98 and 0.50–0.52 for technical and economic performances, respectively. However, the environmental indicators in this range were generally above 0.37, suggesting that a sole focus on technical and economic optimization led to a sharp increase in environmental costs. It is worth noticing that the optimum solution set for the environmental and social double-objective optimization was primarily concentrated in the high range of technical indicators (0.97–0.985) within the four-dimensional space. This indicated that solutions with low pollutant emissions typically relied on higher technical performance, though this came at the cost of economic performance.

Based on the above analysis, the Pareto solution set can be divided into three types: technology-dominated, comprehensive-balanced, and environmentally-friendly. Among them, only the comprehensive-balanced solution set could achieve the optimum solutions that satisfied more than three objectives simultaneously. On the other hand, while excelling in the combination of technical and economic performance, the technology-dominated solution set was relatively weaker in the environmental and social aspects. This indicated that four-dimensional optimization was not merely a simple extension of bi-objective optimization, rather it restructured the relationships between the objectives through higher-dimensional constraints. As a result, the solution set evolved from a planar trade-off to a three-dimensional collaborative optimization, where the interplay between multiple objectives was better accounted for and optimized simultaneously. Additionally, an interesting result was that, in the Pareto front solution set obtained using the 4D-CES, all the solutions corresponded to

Table 10
Relevant parameters for the neural network.

Parameter	Value
ANN	Feedforward Neural Network
Hidden layer number	3
Hidden layer neurons	16/112/48
Activation functions	Hidden/output: ReLU/Linear
Loss function	MSE
Training data division	0.8/0.2

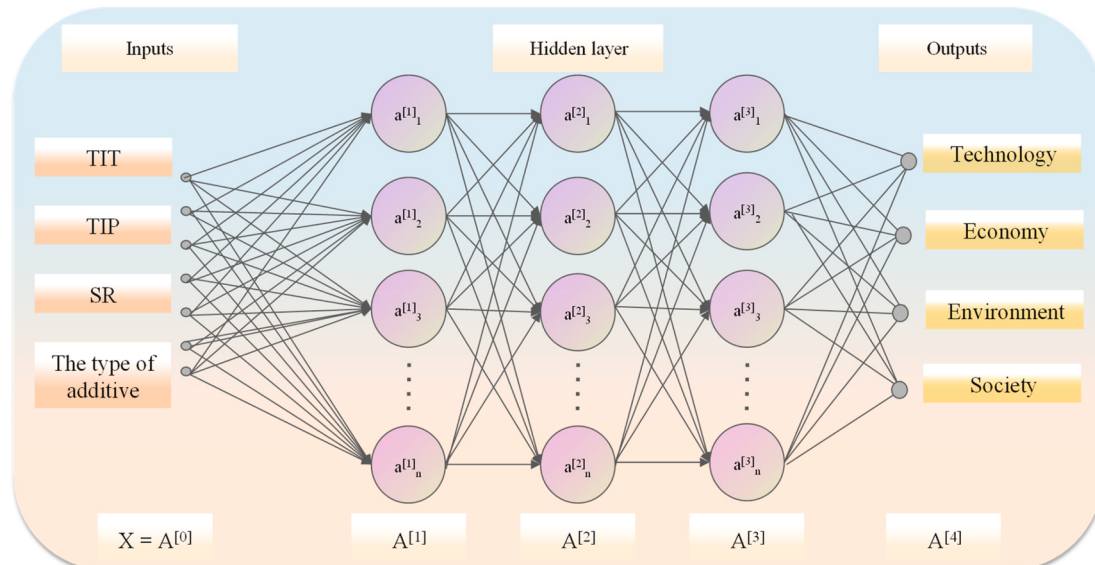


Fig. 7. Artificial neural network Architecture.

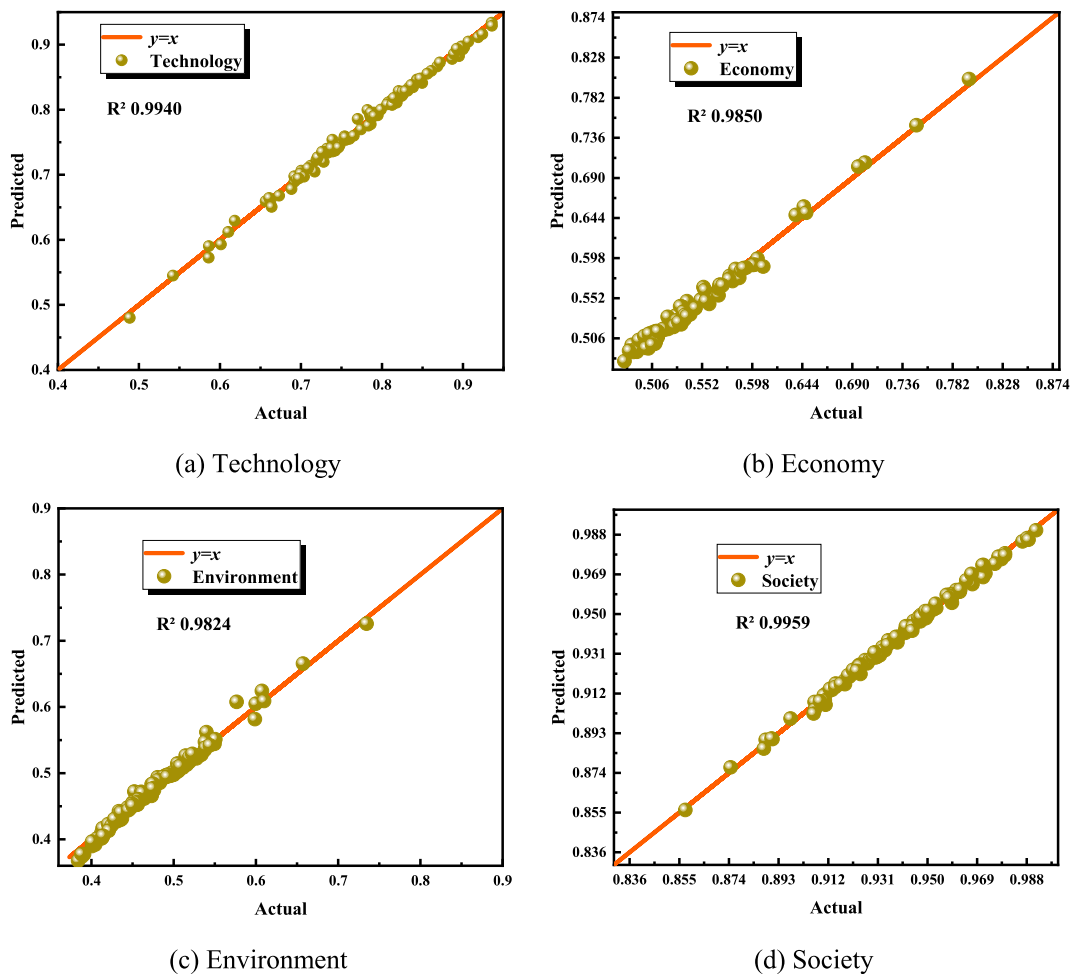


Fig. 8. Verification of the ANN model under different indicators.

Table 11
NSGA-II related operational parameters.

Parameters	Value
Size	500
Generation	500
Crossover	0.9
Mutation	0.1

the additive types of propane and H₂S for the additives of choice. This indicated that, among the five candidate additives, propane and H₂S exhibited significantly comprehensive advantages in the multi-dimensional trade-offs of technical, economic, environmental, and social factors.

3.4. Entropy weight-TOPSIS method

The Pareto front solution set obtained from the surrogate model was used, and the entropy weight method was applied to calculate the weights of different dimensional indicators [36]. The evaluation indicators in the obtained Pareto front solution set were defined as the original evaluation matrix. The original matrix was normalized to achieve dimensionless indicators. The dimensionless forward and inverse indicators are given by Equations (42) and (43), respectively.

$$b_{ij} = \frac{a_{ij,\max} - a_{ij}}{a_{ij,\max} - a_{ij,\min}} \quad (42)$$

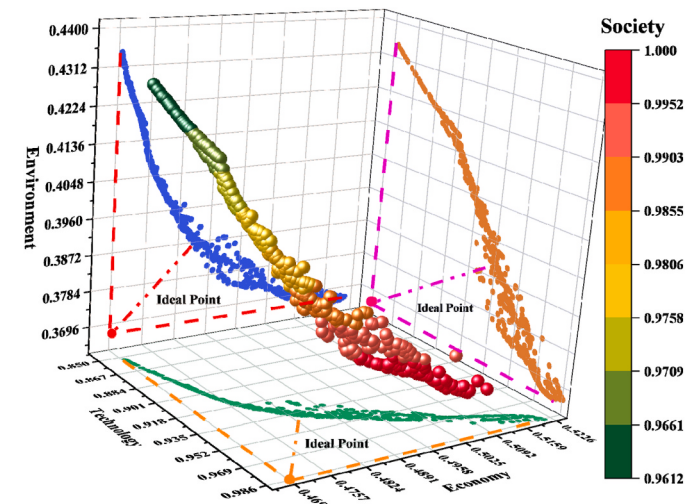


Fig. 9. The distribution of the Pareto front solution set.

$$b_{ij} = \frac{a_{ij,\max} - a_{ij}}{a_{ij,\max} - a_{ij,\min}} \quad (43)$$

where b_{ij} is the element in the normalized matrix.

Subsequently, the information entropy and entropy weights of each indicator are calculated as shown by the data presented in Table 12.

$$e_j = -\frac{1}{In(m)} \cdot \left[\sum_{i=1}^m f_{ij} \cdot Inf_{ij} \right] \quad (44)$$

$$f_{ij} = (1 + b_{ij}) / \sum_{i=1}^m (1 + b_{ij}) \quad (45)$$

$$w_{ij} = \frac{1 - e_j}{\sum_{j=1}^m (1 - e_j)} \quad (46)$$

Fig. 10 shows the weight coefficients of the upper and lower indicators in the entire evaluation system, which are derived using the AHP and the entropy weight method. The results showed that the evaluation system was centered around three main dimensions of technology, economy, and environment, with the social dimension acting as a supplementary factor. Overall, the system presented a multi-dimensional balance with a focus on technology and economic orientation. In the technology dimension, exergy efficiency and thermal efficiency dominated with weights of 48.10 % and 40.50 %, respectively, indicating a double pursuit of both the ‘quality’ and ‘quantity’ in the thermal power conversion process and highlighting that the technical evaluation emphasized the intrinsic performance of the system rather than simply the output capacity. The low weight of specific work was due to its limitations in certain application scenarios. The economic dimension exhibited a similar weight structure, with LCOE and SIC dominating at 48.10 % and 40.50 %, respectively. Overall, they formed a comprehensive evaluation framework that spanned from full lifecycle cost to unit power investment cost. The weight of TCC was 11.40 %, indicating that the evaluation process placed more emphasis on long-term economic viability rather than short-term capital expenditure. In the environmental dimension, the focus was on CO₂ emissions, with PM2.5 emissions serving as a supplementary factor. This was due to CO₂ being the dominant factor in global greenhouse effects, where its reduction was directly related to achieving the ‘double carbon’ goals and fulfilling international climate responsibilities. Moreover, as a typical local pollutant, PM2.5 significantly impact regional air quality and human health. However, their control technologies were relatively mature, and their results were visible in the short term. The social dimension emphasized the number of jobs the system could create. It is worth noticing that the weights of technology and economic dimensions differed by only 0.48 %, which reflected the equal importance of technological innovation and commercial feasibility in the overall evaluation of the system.

After obtaining the entropy weights for each indicator, a weighted decision matrix was constructed, and the comprehensive index for different working fluids in various operating schemes was calculated. Finally, the positive and negative ideal solutions were determined using the Euclidean distance method. Equation (49) was used to calculate the degree of superiority or inferiority of each operating scheme. A value closer to 1 indicated a better evaluation result.

$$\begin{cases} C^+ = \{c_1^+, c_2^+, \dots, c_n^+\} \\ C^- = \{c_1^-, c_2^-, \dots, c_n^-\} \end{cases} \quad (47)$$



Fig. 10. The distribution of double-layer weight.

$$\begin{cases} D_i^+ = \sqrt{\sum_{j=1}^n (c_{ij}^+ - c_{ij})^2} \\ D_i^- = \sqrt{\sum_{j=1}^n (c_{ij}^- - c_{ij})^2} \end{cases} \quad (48)$$

$$O_i = \frac{D_i^-}{D_i^- + D_i^+} \quad (49)$$

where C^+ and C^- represent the positive and negative ideal solution sets, D_i^+ and D_i^- represent the distances between the comprehensive index of the i -th operating scheme and the positive and negative ideal solutions, respectively, and O_i is the relative closeness of the i -th operating scheme. Moreover, the closer the value is to 1, the better the evaluation result for that scheme.

Fig. 11 shows the proximity analysis results of the Pareto front solution set based on the abovementioned method. Among the 500

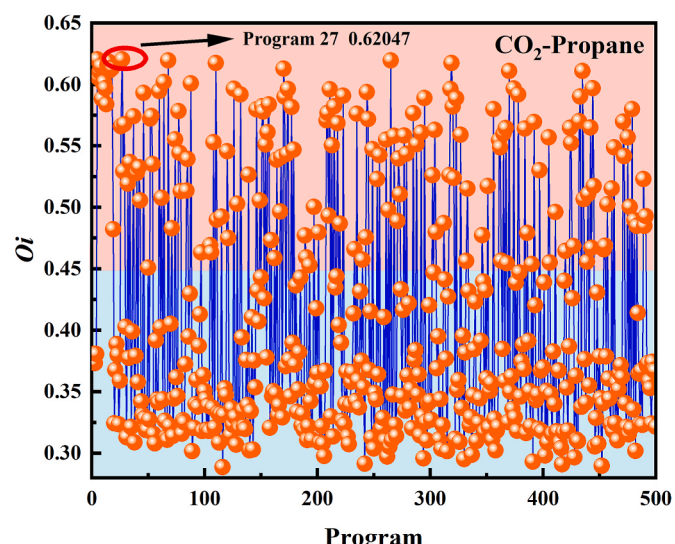


Fig. 11. The relative closeness distribution of different Program.

Table 12
Information entropy and entropy weight results.

Dimension	Information entropy	Entropy weight
Technology	0.9967	0.27714
Economy	0.9964	0.27229
Environment	0.9965	0.25790
Society	0.9975	0.19267

schemes, the relative closeness values showed significant variation, lying within the range of 0.2973–0.6196, with an overall average of 0.407 ± 0.092 . This indicated a clear stratification of performance within the system. This phenomenon was primarily caused by the differences in the types of additives and the operating parameters. It is worth noticing that for the schemes with relative closeness values of more than 0.45, the type of additive consistently came out to be propane, as shown in the orange-shaded area in Fig. 11. This indicated that, under the current weight distribution, the mixed working fluid of CO₂-propane exhibited the best overall performance among the studied working fluids. Additionally, high relative closeness values were often concentrated around specific combinations of operating parameters, suggesting that further improvement in the overall performance could be achieved by optimizing the control of these parameters. Among all the schemes, Program 27 had the highest relative closeness value of 0.62047. This scheme used propane as the additive, whereas the optimum combination of operating parameters was 823.01 K, 26.374 MPa, and 0.226. To further validate the accuracy of the predicted results based on the ANN surrogate model, Program 27 was taken as an example. Moreover, CO₂-propane was chosen as the working fluid, with the turbine's inlet pressure, temperature, and split ratio set to values of 26.374 MPa, 823.01 K, and 0.226 as the input parameters. These values were then substituted into the original mathematical model for further calculations, yielding the results for four indicators. The calculated results were subsequently compared with the predicted values, as shown in Fig. 12. The results showed that the maximum relative error between the calculated and predicted values for the four key indicators was within 1 %, indicating that the model had high predictive accuracy. In particular, the small deviation (0.042 %) between the calculated and predicted values for Indicator 4 demonstrated the excellent predictive capability of the model in the high-value region. However, in the low-value region (such as for Indicator 2), the relative error was slightly higher, which may be related to the distribution of the training data and the model's capability to capture different weight parameters. In summary, the predicted results of the ANN surrogate model were outstanding, exhibiting high accuracy and reliability.

4. Thermodynamic and exergy analyses

The abovementioned results indicated that, compared to pure CO₂, the cycle with CO₂ mixed working fluid demonstrated significant advantages across a multi-dimensional evaluation system, including technical feasibility, economic viability, environmental-friendliness, and social benefits. To further analyze the differences in the performance of system for different working fluids, the present section

conducted a comparative analysis based on the operating parameters obtained above. The section compared key performance indicators of CO₂ and its mixed working fluids under the same operating conditions. Moreover, the perspectives of the distribution of loss in energy and the thermodynamic cycle's T-s characteristics could reveal the fundamental reasons behind the differences among the performances of the system for various working fluids.

4.1. Thermodynamic analysis

Table 13 presents a comparison of the relevant performance of different working fluids under the same operating conditions. The results showed that the mixed working fluid of CO₂-propane exhibited outstanding performance across multiple key indicators. From the perspective of thermodynamic performance, the exergy and thermal efficiencies of CO₂-propane system were 20.44 % and 19.03 %, respectively, which were the highest among the five working fluids studied in the current work. This increased efficiency was primarily attributed to higher carbon-to-hydrogen ratio in the molecular structure of propane [50], as well as its optimized density and specific heat properties as a working fluid, which significantly enhanced the thermal power conversion efficiency of the system. In terms of economic indicators, the CO₂-propane system performed exceptionally well, with an LCOE of only 0.181 \$/kWh, which was 0.014 \$/kWh lower than that of the CO₂ system. This advantage was primarily due to the increased energy output resulting from its higher power generating efficiency. Although the CO₂-propane system did not have the lowest TCC, its SIC was 2394.77 \$/kW, which exhibited a reduction of a 7.31 % compared to the CO₂ system. This indicated that the optimization of the system's compactness effectively reduced the investment for equipment, allowing the CO₂-propane system to offer a better economic return over long term.

With regard to the dimensions of environment and social benefits, the CO₂-propane system also performed exceptionally well. The CO₂ emissions were only 0.139 kg/kWh, showing a reduction of 0.004 kg/kWh compared to the CO₂ system. Moreover, the system could create 103.56 jobs, providing 0.83 more job opportunities than the CO₂ system. Overall, the CO₂-propane system demonstrated significant advantages over other working fluids. Although the initial total investment was slightly higher, its outstanding comprehensive performance made it an ideal choice for applications to thermal energy recovery systems. Not only did it achieve higher energy utilization efficiency, it also reduced operational costs while decreasing environmental burdens. This balance between economic benefits and sustainable development made propane a highly promising additive to working fluids, providing a new technical pathway for the optimization of clean energy systems.

In addition, Fig. 13 shows the distribution of net output power and mass flow rate of working fluid for different working fluids under the same heat source conditions. Under the same heat source conditions, there were significant differences in the net output power and mass flow rate distributions among different working fluids. The CO₂-propane system stood out. The net output power of the system reached 45.185 MW, showing an increase of 1.36 MW compared to the pure CO₂ system, and demonstrating higher energy conversion capability. Meanwhile, the CO₂-propane system had a working fluid mass flow rate of only 430.84 kg/s, which was not only significantly lower than other working fluids but also 25.6 % lower than the pure CO₂ system. This 'high power - low flow' characteristic gave the CO₂-propane system a clear advantage in terms of thermal energy conversion efficiency per unit mass of working fluid. Moreover, the same mass of working fluid could absorb and convert more heat, thereby significantly improving the overall energy efficiency of the system. This excellent feature was due to the synergistic effects of the thermophysical properties of the mixed working fluid of CO₂-propane, which allowed it to utilize the input thermal energy more efficiently during the thermodynamic cycle. This not only reduced load on the system and additional loss of energy caused by excessive flow

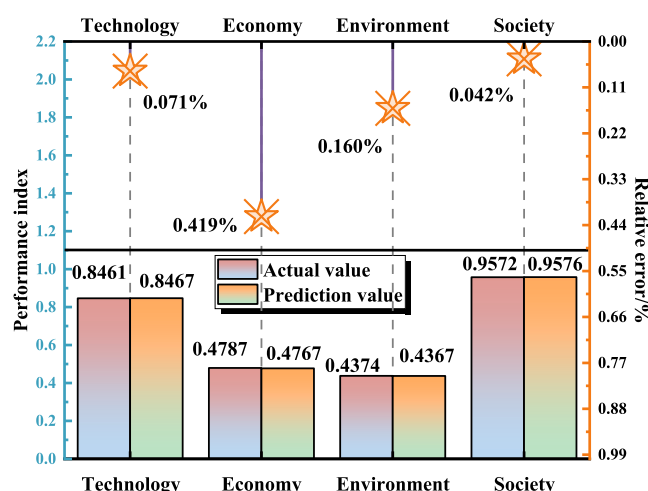
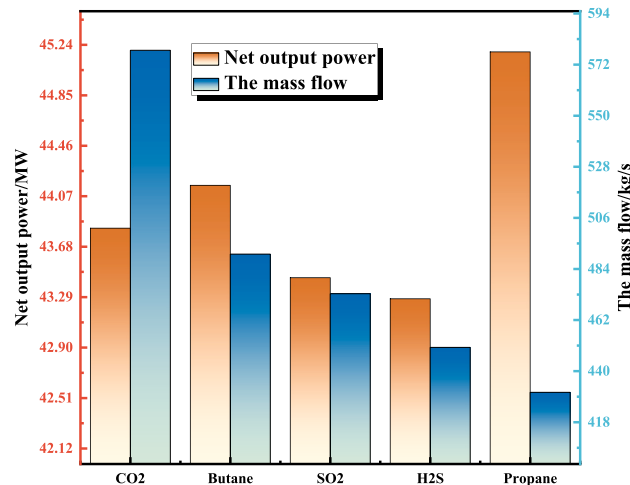


Fig. 12. Comparison between the calculated results and the predicted results.

Table 13

Comparison of key parameters for different working fluids.

Additive	η_{ex}	η_i	W	LCOE	TCC	SIC	CO ₂ _E	PM2.5	JO
CO ₂	19.83	18.46	75.80	0.195	1.13e ⁸	2583.61	0.143	5.02e ⁻⁴	102.73
Butane	19.95	18.60	90.04	0.185	1.08e ⁸	2446.84	0.142	4.99e ⁻⁴	102.93
SO ₂	19.65	18.30	91.78	0.187	1.07e ⁸	2471.89	0.144	5.07e ⁻⁴	102.50
H ₂ S	19.58	18.23	96.13	0.183	1.04e ⁸	2415.03	0.145	5.09e ⁻⁴	102.40
Propane	20.44	19.03	104.88	0.181	1.08e ⁸	2394.77	0.139	4.87e ⁻⁴	103.56

**Fig. 13.** Distribution of net output power and mass flow rate for different working fluids.

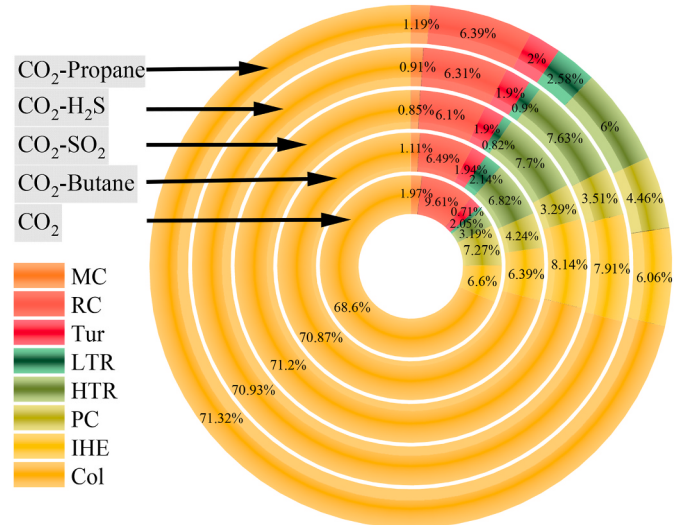
rates but also optimized the thermal power conversion efficiency of the system, which in turn reduced the overall energy losses from the system.

From the perspective of overall energy efficiency, the advantage of CO₂-propane system was not only reflected in its higher power output but also in the lower demand for the working fluid, making it both efficient and economical in the thermodynamic cycle. This characteristic was crucial for enhancing the overall performance of the energy system and provided important insights for the optimization of advanced thermodynamic cycles.

4.2. Exergy analysis

To further clarify the reasons behind the differences in the performance of system employing different mixed working fluids, and to reveal the specific sources and extent of irreversible losses in the thermodynamic system, an exergy analysis was conducted from the perspective of energy losses. The analysis revealed the distribution of irreversible losses for each working fluid within the thermodynamic system. Fig. 14 shows the distribution of exergy losses for different mixed working fluids across various devices.

By comparing the distribution of exergy losses for different mixtures in various devices, it can be observed that the overall advantage of the CO₂-propane system was closely related to its relatively low irreversible losses in key thermodynamic equipment. From the equipment perspective, the collector (Col) served as the main source of exergy loss, accounting for more than 68 % of the total exergy loss in all mixtures, with CO₂-propane system having the highest exergy loss in the collector at 71.32 %. In the HTR, the exergy loss for the CO₂-Propane system was 6.00 %, which was significantly lower than that of the CO₂-SO₂ system (at 7.70 %) and the CO₂-H₂S system (at 7.63 %). This is attributed to its optimized specific heat capacity characteristics, which improve the temperature matching between the working fluid and the heat source in the high-temperature section, thereby reducing the irreversibility of heat transfer. Meanwhile, the exergy loss in the Tur of the CO₂-propane

**Fig. 14.** Exergy loss distribution of different mixtures in various components.

system was 2.00 %, which was slightly higher than that of CO₂-butane system at 1.94 %. Nevertheless, the CO₂-propane system still showed a clear advantage compared to the CO₂ system. This was related to the synergistic effect of the working fluid's density and expansion characteristics. The lower viscosity and higher critical temperature enabled more complete conversion of kinetic energy during the flow process. The results showed that t, among all studied mixtures, the CO₂-propane system had the highest exergy loss of 2.58 % in the LTR. However, this disadvantage was offset by its lower loss in MC, further highlighting the thermophysical advantages of CO₂ and hydrocarbon mixtures in the compression stage [51]. From a system integration perspective, the exergy losses of CO₂-propane system in PC and IHE were 4.46 % and 6.06 %, respectively, which were 2.81 % and 0.54 % lower than those of the CO₂ system. This distribution characteristic indicated that the parameters for the thermodynamic cycle were set closer to the curve for the physical properties of the working fluid, thus effectively reducing the cumulative exergy loss effect during multi-equipment series operation. Particularly, in the optimized combination of TCC and SIC, the mixture further verified the positive impact of a balanced distribution of exergy loss between the equipment on the compactness of the system.

Overall, the CO₂-propane system achieved effective control of exergy loss in equipment with high exergy losses, such as HTR and Tur, by matching its thermophysical parameters with the thermodynamic equipment. Meanwhile, its unique compression performance and heat transfer characteristics balanced the increase in exergy loss in LTR. This ultimately formed the CO₂-propane system's unique 'high power - low flow - low loss' synergistic effect. This was not only the core mechanism behind its improved thermal efficiency but also a crucial foundation for achieving low LCOE and CO₂ emissions.

To further explore differences in the thermodynamic properties of various mixtures, the present section studied the T-s distribution curves of five mixed working fluids throughout the entire thermodynamic cycle, as shown in Fig. 15. The results showed that there was a significant correlation between the thermodynamic cycle characteristics of the

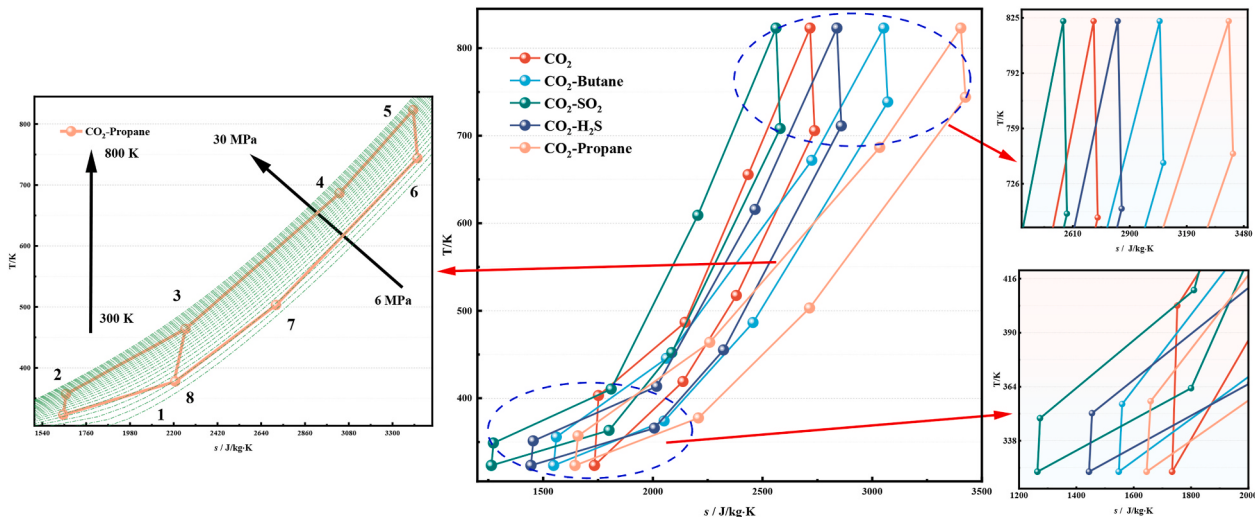


Fig. 15. T-s.

CO_2 -propane mixture and advantages arising from its use. In the high-temperature heat absorption stage (from state Points 3 to 5), the entropy increase of the CO_2 -propane system was significantly higher than those of other mixtures. At the peak temperature of 823 K (Point 5), its entropy reached 3404.25 J/kg·K, exhibiting an increase of 687.37 J/kg·K over that of pure CO_2 system that had a value of 2716.88 J/kg·K. This indicated that the CO_2 -propane mixture had a stronger heat absorption capacity in the high-temperature region. This characteristic stemmed from high carbon-hydrogen ratio and optimized specific heat properties of the molecular structure of propane, which better matched the temperature difference between the working fluid and the heat source, thus reducing the irreversible heat transfer losses in HTR. In the expansion work stage (from Points 5 to 6), the entropy of the CO_2 -propane system increased only by 0.6 %, while the entropy increase of the pure CO_2 system was 0.85 %. This indicated that the expansion process in Tur for the CO_2 -propane system was closer to an isentropic state, resulting in higher energy conversion efficiency. This also explained why the energy loss in the turbine of the CO_2 -propane system was 2.00 %, which was 0.05 % lower than that of the pure CO_2 system.

In the low-temperature heat rejection stage (from Points 6 to 8), although the entropy of the CO_2 -propane system was higher, its temperature gradient was more gradual, which helped control the loss in the quality of energy caused by fluid's subcooling in the heat exchanger. Moreover, during the compression process (from Points 1 to 2), the increase in the entropy of CO_2 -propane mixture was only 14.12 J/kg·K, which was significantly lower than the value of 18.09 J/kg·K for the pure CO_2 system. This advantage was due to the weaker intermolecular forces in the CO_2 -propane mixture, which reduced the work required for compression that was directly reflected in the main compressor's energy loss of only 1.19 %. Interestingly, the CO_2 -propane system exhibited a relatively high entropy increase in the low-temperature regenerator. However, this disadvantage was balanced by its efficient heat absorption in the high-temperature section and low-loss characteristics during the compression process, resulting in a distinct 'high-temperature energy storage enhancement - low-temperature controllable energy release' feature. This thermodynamic characteristic, coupled with the deep adaptation of its physical properties, not only boosted the thermal efficiency of CO_2 -propane system to 19.03 %, but also optimized the system's compactness by reducing irreversible losses in key equipment. Ultimately, this resulted in significant advantages for the thermal performance, economic efficiency, and environmental characteristics, further emphasizing the core role of the optimization of thermodynamic parameters in enhancing the overall performance of the system.

4.3. Discussion

The thermodynamic and exergy analyses revealed the collaborative optimization mechanism of the CO_2 -propane system, which was characterized by 'high power - low flow resistance - low losses.' However, this result fundamentally stemmed from the innovative breakthrough of the methodology proposed in the current study. The double-helix weighting mechanism precisely quantified the advantageous physical properties of propane. The ANN surrogate model enabled the rapid determination of its optimum operating conditions. Compared to existing research, the present study achieved a breakthrough in methodology through the completeness of the evaluation system, the efficiency of ANN surrogate model, and the reliability of the decision-making process. Moreover, the present study provides new insights for the optimization of mixed working fluid-based solar thermal power generating systems.

As shown by the data presented in Table 14, compared to the commonly used thermodynamic-economic single-objective optimization models in contemporary research (such as those by [13], Cheng [14], Dai [15], which only focus on the trade-off between thermal efficiency and LCOE), the present study innovatively constructed a comprehensive evaluation system (4D-CES) that included four dimensions of technology, economy, environment, and society. This

Table 14
Comparison of the proposed method with those reported in the literature.

	Traditional Methods	Current work	Advantages
Completeness of the Evaluation System	Thermodynamic and Economic Single-Objective Optimization (such as Ma [13], Cheng [14], and Dai [15])	Four-Dimensional Comprehensive Evaluation System	Evaluation of Technology, Economy, Environment, and Social Indicators
Efficiency of the ANN Surrogate Model	Enumeration Method [18], Face-Centered Cubic Design [52]	ANN Surrogate Model	The computational cost is significantly reduced,
Reliability of the Decision-Making Process	AHP Method [42]	Double-Helix Weighting Mechanism (AHP-Entropy Weight Method)	It significantly enhances the scientific accuracy and reliability of complex energy system decision-making.

groundbreaking design not only filled the gap in the quantitative assessment of non-technical indicators in existing research but also, through the allocation of scientific weights shown in Table 9 and Fig. 10, achieved the multi-objective collaborative optimization of solar thermal power generating system for the first time.

At the same time, traditional parameter optimization methods (such as the enumeration method used by Xu et al. [18] and the face-centered cubic design used by Cao et al. [52]) typically require a much larger number of simulations. In contrast, the ANN surrogate model only requires 500 data sets for each working fluid. With a prediction error of less than 1 % (as validated by the data shown in Fig. 12), it significantly reduces computational costs. This significant improvement in computational efficiency enables the NSGA-II algorithm to generate a high-quality Pareto front solution set within a reasonable time, providing a practical and feasible optimization tool for engineering applications.

In addition, to address the inherent flaws of the traditional AHP method (such as strong subjectivity and unreasonable allocation of weights [42]), an innovative double-helix weighting mechanism is proposed. By coupling AHP with the entropy weight method (Section 3.4), the consistency ratio is strictly controlled within a reasonable range. The entropy weight method is used to objectively correct the initial weights (Table 12), effectively eliminating the subjective bias. As a result, the closeness of the CO₂-propane system reaches 0.62047, significantly outperforming other working fluids.

5. Conclusions

This paper innovatively proposes a double-spiral weighting mechanism and utilizes artificial neural networks to construct a surrogate model for solar thermal power generating system employing CO₂ mixed working fluids. It establishes a multidimensional comprehensive evaluation system focusing on technology, economy, environment, and social responsibility. Within the proposed system, the optimization of the solar thermal power generating system's overall performance is achieved through the selection of additives and the determination of operating parameters. Furthermore, from the perspectives of thermodynamics and energy loss, the deep-rooted reasons behind differences in the performances of mixed working fluids are revealed, providing both theoretical support and practical solutions for the optimization of the overall performance of the system. The main conclusions are as follows.

- (1) By integrating multidimensional indicators through the double-spiral weighting mechanism, a 4D-CES evaluation system was established. Combined with the ANN surrogate model and the NSGA-II optimization algorithm, the computational complexity was reduced. The multi-objective prediction indicated that, when the technical performance was optimized, it led to a 50 % increase in economic costs and a 37 % increase in environmental burden. Additionally, errors in the predictions of surrogate model were less than 1 %, further confirming the reliability of ANN surrogate model.
- (2) The CO₂-propane system stood out among various mixed working fluids with high closeness of 0.62047. The corresponding inlet pressure and temperature of turbine, and split ratio were 26.374 MPa, 823.01 K, and 0.226, respectively. Moreover, in the operational schemes with high closeness, all selected additives were propane, whereas the operating parameters were concentrated within a specific range. This result indicated that by optimally selecting propane as the additive and precisely controlling the operating parameters, the overall performance of the system can be significantly improved.
- (3) The CO₂-propane system demonstrated various advantages in terms of its performance. Compared to the CO₂ system, the η_i increased by 0.57 %, whereas W_{net} is 45.185 MW, indicating an increase of 1.36 MW. The mass flow rate was only 430.84 kg/s,

showing a clear 'high power - low flow' characteristic. In terms of economics, the LCOE and SIS also showed significant advantages, with values of 0.181 \$/kWh and 2394.77 \$/kW, respectively. The system achieved a synergistic optimization of high thermal power conversion efficiency and economic returns, making it an ideal choice for thermal energy recovery systems.

- (4) The CO₂-propane system significantly reduced irreversible losses in key equipment by optimizing the matching of physical properties with the equipment. Its η_{ex} increased to 20.44 %, which was 0.61 % higher than that of the pure CO₂ system. Despite higher generation of entropy in LTR, the system demonstrated a 'high power - low flow - low loss' synergistic effect, which was due to the low-loss performance of MC and the optimized performance in the high-temperature section. This optimization improved the system's compactness and enhanced its overall performance.

Nomenclature:

A	Area (m ²)
C	Ideal solution set
D	Euclidean distance
N	Type of additive
E	Exergy
O	Relative closeness value
P	Pressure (MPa)
Q	Heat Transfer Rate (kW)
U	Heat transfer coefficient (W/(m ² K))
T	Temperature (K)
t	Operating hours (h)
W	Power (kW)
Z	Investment cost
f _c	Friction factor
h	specific enthalpy (kJ·kg ⁻¹)
i	Interest rate
k	Component
m	Mass Flow Rate (kg s ⁻¹)
Greek letters:	
λ	Thermal conductivity (W/(m·K))
δ	Thickness (m)
η	Efficiency (%)
θ	Incidence angle of the solar beam (°)
Re	Reynolds number
Nu	Nussel number
Pr	The Prandtl number
Subscripts and abbreviations:	
Ambt	Ambient temperature (K)
AHP	Analytic hierarchy process
ANN	Artificial neural network
CES	Comprehensive Evaluation System
CEPCI	Chemical Engineering Plant Cost Index
CI	Consistency Index
CO ₂ _E	Emissions of CO ₂
C _p	Specific heat capacity (kJ/kg)
CR	Consistency ratio
CRF	Cost recovery factor
CSP	Concentrated Solar Power plant
D _h	The hydraulic diameter
DNI	Direct Normal Irradiation (W/m ²)
HTF	Heat Transfer Fluid
HTR	High-Temperature Recuperator
IHE	Intermediate heat exchanger
JO	Job opportunities
LCOE	Levelized Cost of Electricity
LT	Operation life
LTR	Low-Temperature Recuperator
MC	Main Compressor
MSE	Mean Squared Error
ORC	Organic Rankine cycle
PC	Precooler
PM2.5_E	Emissions of PM2.5
PR	Pressure Ratio
RC	Re-Compressor

(continued on next page)

(continued)

RI	Random Consistency Index
Salt	Molten salt
SPT	Solar power tower
SR	Split Ratio
SIC	Specific Investment Cost
TCC	Total Capital Cost
TDC	Total direct cost
TES	Thermal Energy Storage
TIC	Total indirect cost
TIT	Turbine Inlet Temperature
TIP	Turbine Inlet Pressure
Tur	Turbine
charge	The charge time.
cold	cold fluid
Col	collector
com	compressor
discharge	the discharge time
ele	Emissions during electricity consumption
ex	Exergy efficiency
hot	hot fluid
in	inlet
mat	Emissions during the construction
max	Maximum value
min	Minimum value
net	net power output
out	outlet
pc	Power cycle efficiency
sCO ₂	Supercritical Carbon Dioxide
tol	Total emissions

CRediT authorship contribution statement

Qingqiang Meng: Writing – original draft, Visualization, Methodology, Investigation, Data curation. **Lihua Cao:** Funding acquisition, Conceptualization. **Yanchao Li:** Writing – review & editing. **Heyong Si:** Writing – review & editing, Funding acquisition. **Yaoli Wang:** Writing – review & editing. **Feng Hou:** Writing – review & editing.

Declaration of competing interest

The authors declare that they have no known competing financial interests or personal relationships that could have appeared to influence the work reported in this paper.

Acknowledgment

The authors gratefully acknowledge the support from the National Natural Science Foundation of China (No. 52206004).

Data availability

No data was used for the research described in the article.

References

- [1] Ehsan MM, Awais M, Lee S, Salehin S, Guan Z, Gurgenci H. Potential prospects of supercritical CO₂ power cycles for commercialisation: applicability, research status, and advancement. Renew Sustain Energy Rev 2023;172:113044.
- [2] Deng Q, Liu A, Li J, Feng Z. A review on supercritical CO₂ and CO₂-based mixture in power cycle. Energy Convers Manag 2025;324:119295.
- [3] Ehsan MM, Guan Z, Gurgenci H, Klimenko A. Feasibility of dry cooling in supercritical CO₂ power cycle in concentrated solar power application: review and a case study. Renew Sustain Energy Rev 2020;132.
- [4] Cao L, Meng Q, Fang M, Si H. Thermo-economic comprehensive evaluation of a CO₂-based mixed working fluid concentrated solar power system via WOA-AHP approach. Therm Sci Eng Prog 2025;103863.
- [5] Bian X, Wang X, Wang J, Wang R, Zhang X, Tian H, et al. Transcritical CO₂ mixture power for nuclear plant application: concept and thermodynamic optimization. Energy 2024;309.
- [6] Ma N, Meng F, Hong W, Li H, Niu X. Thermodynamic assessment of the dry-cooling supercritical brayton cycle in a direct-heated solar power tower plant enabled by CO₂-propane mixture. Renew Energy 2023;203:649–63.
- [7] Niu X, Ma N, Bu Z, Hong W, Li H. Thermodynamic analysis of supercritical brayton cycles using CO₂-based binary mixtures for solar power tower system application. Energy 2022;254.
- [8] Illyés VC, Di Marcoberardino G, Werner A, Haider M, Manzolini G. Experimental evaluation of the CO₂-based mixture CO₂/C6F₆ in a recuperated transcritical cycle. Energy 2024;313.
- [9] Lang L, Fu Y, Jiang F, Cheng K, Wang C, Dang C, et al. Investigation the thermodynamic performance of closed brayton cycle with CO₂-based binary mixtures for hypersonic vehicle power generation systems under finite cold source. Therm Sci Eng Prog 2025;63.
- [10] Luo Y, Su Z, Li Z, Zheng N, Wei J. Off-design performance analysis of supercritical CO₂ mixture brayton cycle with floating critical points. Sol Energy 2024;276.
- [11] Liang Y, Zhu Y, Liang G, Liang Y, Ling X. Comprehensive analysis and optimization of a novel solar-driven two-stage condensation transcritical power system using CO₂-based mixture for liquefied natural gas cold energy recovery. Energy 2025;332.
- [12] Tang J, Li Q, Werle S, Wang S, Yu H. Development and comprehensive thermo-economic analysis of a novel compressed CO₂ energy storage system integrated with high-temperature thermal energy storage. Energy 2024;303.
- [13] Ma Y-N, Hu P, Jia C-Q, Wu Z-R, Chen Q. Thermo-economic analysis and multi-objective optimization of supercritical brayton cycles with CO₂-based mixtures. Appl Therm Eng 2023;219.
- [14] Cheng Y, Hu W, Pei Z. Multi-objective optimization of CO₂-based mixtures for supercritical brayton cycle: balancing thermodynamic, economic, and compactness criteria. Appl Therm Eng 2025;278.
- [15] Dai B, Wang Q, Liu S, Zhang J, Wang Y, Kong Z, et al. Multi-objective optimization analysis of combined heating and cooling transcritical CO₂ system integrated with mechanical subcooling utilizing hydrocarbon mixture based on machine learning. Energy Convers Manag 2024;301:118057.
- [16] Yang M-H. The performance analysis of the transcritical rankine cycle using carbon dioxide mixtures as the working fluids for waste heat recovery. Energy Convers Manag 2017;151:86–97.
- [17] Khan TE, Sakib SH, Sakib N, Hossain T, Ehsan MM, Khan Y. Multi-objective optimization of a cascaded supercritical CO₂ brayton cycle with ejector-enhanced transcritical CO₂ and flash tank absorption refrigeration cycles. Energy Convers Manag X 2025;26.
- [18] Xu X, Wu C, Liu C, Xu X. Feasibility assessment of trough concentrated solar power plants with transcritical power cycles based on carbon dioxide mixtures: a 4E analysis and systematic comparison. J Clean Prod 2024;436.
- [19] Li P, Molina E, K W, X X, G D, A K. Thermal and transport properties of NaCl-KCl-ZnCl₂ eutectic salts for new generation high temperature heat transfer fluids. J Sol Energy Eng 2016;138.
- [20] Desai NB, Bandyopadhyay S, Nayak JK, Banerjee R, Kedare SB. Simulation of 1MWe solar thermal power plant. Energy Proc 2014;57:507–16.
- [21] Burhanuddin Halimi KYS. Computational analysis of supercritical CO₂ brayton cycle power conversion system for fusion reactor. Energy Convers Manag 2012;63:38–43.
- [22] AlZahrani AA, Dincer I. Energy and exergy analyses of a parabolic trough solar power plant using carbon dioxide power cycle. Energy Convers Manag 2018;158:476–88.
- [23] Ata D, Akbari SMSM. Thermoeconomic analysis & optimization of the combined supercritical CO₂ (carbon dioxide) recompression brayton/Organic rankine cycle. Energy 2014;78:1–12.
- [24] Chemical engineering - Chemical engineering essentials for the global chemical processing industries (CPI) n.d. <https://www.chemengonline.com/> (accessed February 5, 2023).
- [25] Mahmoudi S S, Salehi S, Yari M, Rosen M. Exergoeconomic performance comparison and optimization of single-stage absorption heat transformers. Energies 2017;10(4).
- [26] Ghaebi H, Amidpour M, Karimkashi S, Rezayan O. Techno-economic study on compact heat exchangers. Int J Energy Res 2011;32(12):697–1127. 1119–1127.
- [27] Guo-Yan Z, En W, Shan-Tung T. Techno-economic study on compact heat exchangers. Int J Energy Res 2008;32(12):1119–27.
- [28] Mokhtari Shahdost B, Jokar MA, Razi Astaraei F, Ahmadi MH. Modeling and economic analysis of a parabolic trough solar collector used in order to preheat the process fluid of furnaces in a refinery (case study: Parsian gas refinery). J Therm Anal Calorim 2019;137(6):2081–97.
- [29] Zhou Y, Han X, Wang D, Sun Y, Li X. Optimization and performance analysis of a near-zero emission SOFC hybrid system based on a supercritical CO₂ cycle using solar energy. Energy Convers Manag 2023;280.
- [30] Wu C, Wang S-s, Feng X-j, Li J. Energy, exergy and exergoeconomic analyses of a combined supercritical CO₂ recompression Brayton/absorption refrigeration cycle. Energy Convers Manag 2017;148:360–77.
- [31] Hu L, Chen D, Huang Y, Li L, Cao Y, Yuan D, et al. Investigation on the performance of the supercritical Brayton cycle with CO₂-based binary mixture as working fluid for an energy transportation system of a nuclear reactor. Energy 2015;89:874–86.
- [32] Jing Y-Y, Bai H, Wang J-J, Liu L. Life cycle assessment of a solar combined cooling heating and power system in different operation strategies. Appl Energy 2012;92:843–53.
- [33] Ren F, Wang J, Zhu S, Chen Y. Multi-objective optimization of combined cooling, heating and power system integrated with solar and geothermal energies. Energy Convers Manag 2019;197:111866.
- [34] Wang J, Yang Y, Mao T, Sui J, Jin H. Life cycle assessment (LCA) optimization of solar-assisted hybrid CCHP system. Appl Energy 2015;146:38–52.
- [35] Cameron L, Bvd Zwaan. Employment factors for wind and solar energy technologies: a literature review. Renew Sustain Energy Rev 2015;45:160–72.

- [36] Chen Y, Wang J, Lund PD. Sustainability evaluation and sensitivity analysis of district heating systems coupled to geothermal and solar resources. *Energy Convers Manag* 2020;220.
- [37] Campos-Guzmán V, García-Cáscales MS, Espinosa N, Urbina A. Life cycle analysis with Multi-Criteria Decision Making: a review of approaches for the sustainability evaluation of renewable energy technologies. *Renew Sustain Energy Rev* 2019;104:343–66.
- [38] Xu Z, Liu X, Xie Y. Off-design performances of a dry-cooled supercritical recompression Brayton cycle using CO₂-H₂S as working fluid. *Energy* 2023;276.
- [39] Ren Shaoran, Haikui Li, Leibing Li. An experimental study of effects of inert and special flammable gases on methane's explosion characteristics. *Nat Gas Ind* 2013; 33(10):110–5.
- [40] Liu X, Xu Z, Xie Y, Yang H. CO₂-based mixture working fluids used for the dry-cooling supercritical brayton cycle: thermodynamic evaluation. *Appl Therm Eng* 2019;162.
- [41] Tafur-Escanta P, López-Paniagua I, Muñoz-Antón J. Thermodynamics analysis of the supercritical CO₂ binary mixtures for brayton power cycles. *Energy* 2023;270.
- [42] Al-Awadhi T, Al Ramimi W, Al Jabri K, Abulibdeh A. Solar farms suitability analysis using GIS-based analytic Hierarchy Process (AHP) multi-criteria: a case study of Al Duqm – oman. *Renew Energy* 2025;241.
- [43] Ullah A, Mahmood M, Iqbal S, Sajid MB, Hassan Z, AboRas KM, et al. Techno-economic and GHG mitigation assessment of concentrated solar thermal and PV systems for different climate zones. *Energy Rep* 2023;9:4763–80.
- [44] Valencia G, Fontalvo A, Duarte Forero J. Optimization of waste heat recovery in internal combustion engine using a dual-loop organic Rankine cycle: Thermo-economic and environmental footprint analysis. *Appl Therm Eng* 2021;182.
- [45] Mohideen MM, Ramakrishna S, Prabu S, Liu Y. Advancing green energy solution with the impetus of COVID-19 pandemic. *J Energy Chem* 2021;59:688–705.
- [46] Zhu H, Xie G, Berrouk AS. Enhancing performance of multi-pressure evaporation organic Rankine Cycle/Supercritical Carbon Dioxide Brayton cycle through genetic algorithm and Machine learning optimization. *Energy Convers Manag* 2024;301.
- [47] Ruiz-Casanova E, Rubio-Maya C, Ambriz-Díaz VM, Gutiérrez Martínez A. Energy, exergy and exergoeconomic analyses and ANN-based three-objective optimization of a supercritical CO₂ recompression Brayton cycle driven by a high-temperature geothermal reservoir. *Energy* 2024;311.
- [48] Deb K, Member A, Pratap A, Agarwal S, Meyarivan T. A fast and elitist multiobjective genetic Algorithm: NSGA-II. *IEEE Trans Evol Comput* 2022;6: 182–97.
- [49] Feng SGQA. Application of fast and elitist non-dominated sorting generic algorithm in multi-objective reactive power Optimization. *Trans China Electrotech Soc* 2007; 22(12):146–51.
- [50] Moradi H, Azizpour H, Mohammadi M. Study of adsorption of propane and propylene on CHA zeolite in different Si/Al ratios using molecular dynamics simulation. *Powder Technol* 2023;419.
- [51] Meng Q, Cao L, Fang M, Si H. Dynamic response characteristics of sCO₂ mixtures under variable conditions. *Energy* 2025;315.
- [52] Yue C, Ranjing C, Jun Z, Yifan C, Fengqi S. Rapid prediction and optimization for off-design performance of gas and supercritical carbon dioxide combined cycle based on neural network. *Proceedings of the CSEE* 2023;43.